Proceedings of the ASME 2017 International Mechanical Engineering Congress and Exposition
IMECE2017
November 3-9, 2017, Tampa, Florida, USA

IMECE2017-70143

MOLECULAR DYNAMICS INVESTIGATION OF PHASE CHANGE INDUCED BY ULTRAFAST LASER IRRADIATION

Pengfei Ji and **Yiming Rong**
Department of Mechanical and Energy Engineering
Southern University of Science and Technology
Shenzhen 518055, China

Yuwen Zhang
Department of Mechanical and Aerospace Engineering
University of Missouri
Columbia MO 65211, USA

Yong Tang
Key Laboratory of Surface Functional Structure Manufacturing of Guang Dong Higher Education Institutes
School of Mechanical and Automotive Engineering
South China University of Technology
Guangzhou 510640, China

ABSTRACT

Irradiated by ultrafast laser pulse, the phase change phenomena in aluminum film are investigated via molecular dynamics simulation. The embedded-atom method potential is employed to describe atomic interactions. The laser heating is modeled by adding a kinetic energy term to the laser pulse irradiated atom at each time step. The resolidification is realized by thermal conduction to cool down locally melted atoms. The temporal and spatial distribution of atomic motion is recorded to compute the temperature evolution and structure change during melting and resolidification processes. The interface between solid and liquid is identified via Ackland analysis. Due to the temperature difference, diffraction profile of the resolidified aluminum is found different from the aluminum before laser irradiation. The simulation results provide helpful information on the atomic scale temperature variation and structure transformation underlying ultrafast laser induced phase change.

INTRODUCTION

The implementation of ultrafast laser material processing has appealed considerable interests in the past decades [1–5]. Comparing with nanosecond laser and continuous wave laser in micromachining, ultrafast laser owns the merits of highly localized material removal, little heat affected zone, and small collateral damage [6]. For the purpose of achieving desired result after ultrafast laser processing of metallic material, to grasp the detailed mechanism underlying phase change phenomena becomes essential.

Complex multiphysical processes involving thermal nonequilibirum, heat conduction, thermal stress propagation and microstructural variation are triggered upon ultrafast laser irradiation [6–13]. Conventional continuum approach encounters limitation in describing ultrafast and extreme laser heating problems. Whereas, molecular dynamics (MD) simulation is free from the prerequisites of macroscopic material parameters. During MD simulation, microscopic scene is captured via atomic motion and trajectory. Thereby, MD simulation owns a capability to discover the mechanism determining thermophysical phenomena occurring during ultrafast laser material interactions [14]. Ultrafast laser interaction with aluminum has been seen in [14–19]. Nevertheless, to the best of the authors' knowledge, MD work focusing on ultrafast laser induced phase change from melting to resolidication, as well as the structure change of laser irradiated material is still not reported. This paper paves a novel way to capture the scenes from ultrafast laser melting to resolidification.

NOMENCLATURE

E	Energy, J
F	Embedding energy, J
g	Pair correlation function
I	Source term of the laser energy, W/m^3
J	Laser fluence, J/m^2

L Laser penetration depth, m
q Scattering factor
r Position of an atom, m
S Structure factor
t Time, s
T Temperature, K
U Interatomic potential, J
V Volume, m^3

Greek Letters

α Atom type 1
β Atom type 2
ρ Number density
ϕ Pair function

Subscripts and Superscripts

abs Absorption
k Kinetic energy
op Optical property
p Pulse

MODELING AND SIMULATION

An aluminum film with thickness of $150\ nm$ was prepared at room temperature ($300\ K$) before laser irradiation. The computational domain was set as $200\ nm$ in x-direction and $1.62\ nm$ in y- and z-directions. The ultrafast laser pulse irradiates along x-direction. Periodic boundary conditions were imposed in y- and z-directions. Free boundary conditions were applied on the front and rear surfaces of the silver film in x-direction. There were two empty spaces in front and behind the aluminum film, allowing laser induced thermal expansion. A schematic view of the modeled system is seen in Fig. 1.

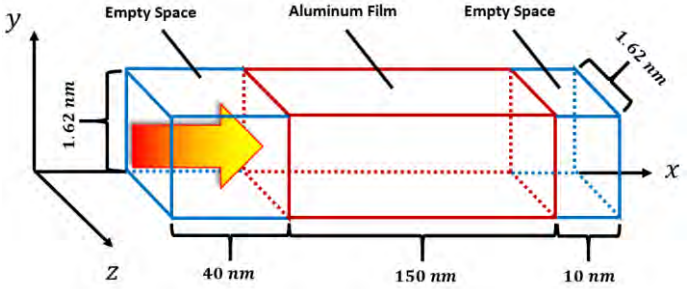

Fig. 1 Schematic illustration of the modeled system.

The interatomic motion was governed by Newton's second law, force of which was calculated from spatial derivative of interatomic potential. The initial atomic configuration and dynamic vibration were generated to obey a Gaussian distribution with a mean value of 0.0 and a sigma scaled to meet $300\ K$. The velocity form of the Verlet algorithm was implemented to integrated Newton's equation of motion [20]. The embedded atom method (EAM) potential for aluminum was adopt in MD simulation [21]. The energy U_i of each atom i in EAM potential is expressed as

$$U_i = F_\alpha\left[\sum_{i\neq j}\rho_\beta(r_{ij})\right] + \frac{1}{2}\sum_{i\neq j}\phi_{\alpha\beta}(r_{ij}), \quad (1)$$

where F is the embedding energy needed to place atom i of type α into an electron cloud. The contribution of electron charge density from atom j of type β at location of atom i is denoted as ρ_β. The pair function is $\phi_{\alpha\beta}$. The element types of atoms i and j are denoted as α and β, respectively. The distance between atoms i and j is r_{ij}

The MD simulation was divided into three stages with a total length of $5\ ns$. The first stage was to prepare the aluminum film at equilibrium at $300\ K$, which lasted for $0.5\ ns$ as a canonical NVT ensemble. The Nose-Hoover thermostat was adopted to equilibrate the system [22]. The second stage was laser irradiation process with a temporal period lasting for $0.1\ ns$. The third stage lasted for $4.4\ ns$, which was simulated in terms of microcanonical NVE ensemble to let locally heated zone get thermal equilibrium with remained cold zone. The framework of computation was carried out by developing a functional extension (laser material interaction module) on the basis of the LAMMPS software package [23].

Transportation of laser energy from the laser irradiated surface to the deeper side of aluminum film obeys the Beer-Lambert law. Namely, the laser intensity decays exponentially from the front surface, which is expressed as

$$S(x,t) = \frac{0.94J_{abs}}{t_p L_{op}} exp(-\frac{x}{L_{op}}) exp[-2.77\frac{(t-t_0)^2}{{t_p}^2}], \quad (2)$$

where J_{abs} is the absorbed laser fluence. The optical penetration depth L_{op} was $8\ nm$ [14], which was used to represent the range of laser energy deposition. The full width at half maximum (FWHM) was $500\ fs$, which denoted laser pulse duration t_p. The temporal center point of laser beam t_0 located at $0.55\ ns$, which ensured the laser intensity decayed to 0 at the beginning ($0.5\ ns$) and end ($0.6\ ns$) of the second stage.

The laser energy deposition at give position x and time t was modeled by adding a non-translational kinetic energy to the laser irradiated group of atoms in a way conserving their aggregate momentum. In order to convert the laser intensity to the added kinetic energy, $S(x,t)$ was multiplied the MD time step Δt ($1\ fs$) and the average volume V_i that atom i occupied, namely

$$E_k(t+\Delta t) = E_k(t) + S(x,t)\Delta t V_i. \quad (3)$$

The effect of statistical error induced by MD simulation was examined by carrying out six parallel cases, which set different seeds for numerical generators to initialize the modeled system in Fig. 1. The calculated temperatures at $5\ ns$ (after resolidification) were $386.22\ K$, $386.12\ K$, $388.24\ K$, $387.60\ K$, $386.52\ K$ and $385.59\ K$, respectively, which demonstrated there were no significant differences among the six cases. Thereby, the first case was chosen as a typical case representing the phase changes from laser melting to resolidification.

RESULTS AND DISCUSSION

Temporal and Spatial Evolution of Temperature

Figure 2 shows evolution of temperature when the modeled aluminum film is irradiated by a laser pulse with absorbed fluence of $0.05\ J/cm^2$. The second stage during laser irradiation and third stage after laser irradiation are shown in Figs. 2(a) and 2(b), respectively. Temperature distribution at

0.5 ns presents a horizontal profile around 300 K, indicating well thermal equilibration achieved from the first stage of preparation. An abrupt temperature increase is seen at 0.55 ns, when the laser intensity evolves to the peak. It should be noted that the depth of locally heated region is around 8 nm at 0.55 ns, which equals to the optical penetration depth [14] in Eq. (2) and proves the validity of the programmed laser absorption process in this paper.

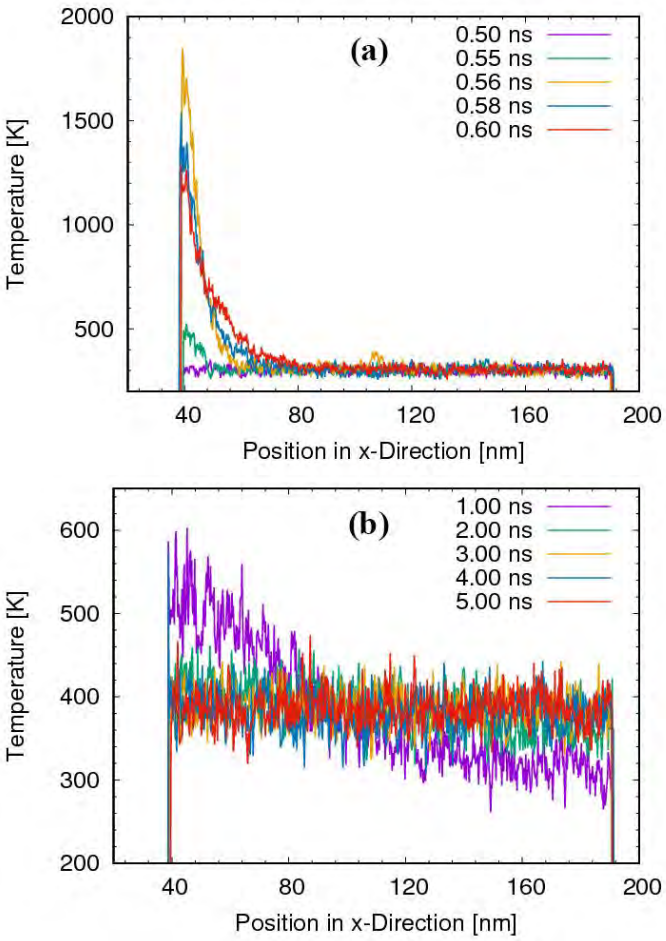

Fig. 2 Temporal and spatial evolution of temperature. (a) The laser irradiation stage from 0.5 ns to 0.6 ns. (b) The stage after laser irradiation until 5 ns. (For the best interpretation of the calculated results, color version of this figure is seen online.)

With the going on of simulation, laser energy has been completely deposited into a shallow region below the front surface of the aluminum film. Temperature reaches a value as high as 1846 K at 0.56 ns. Accompanying with the laser heating, thermal conduction propagates from the locally heated front region to the rear cold region. As seen in Fig. 2(b), temperature in the film renders uniform distribution slightly lower than 400 K from 3.00 ns to 5.00 ns, which demonstrates a finally thermal equilibrium state has been obtained. The average temperature calculated at 5.00 ns is 386.22 K, which indicates the energy absorption of incident laser pulse leading to the overall increase of temperature.

Melting and Resolidification from Ackland Analysis

One of the primary goals of this paper is to investigate ultrafast laser induced solid-liquid melting and subsequent liquid-solid resolidification processes. Local structure analysis was perform by utilizing the formulation given by Ackland [24]. The method is based on angles between atoms rather than their distance, which is stable against temperature boost.

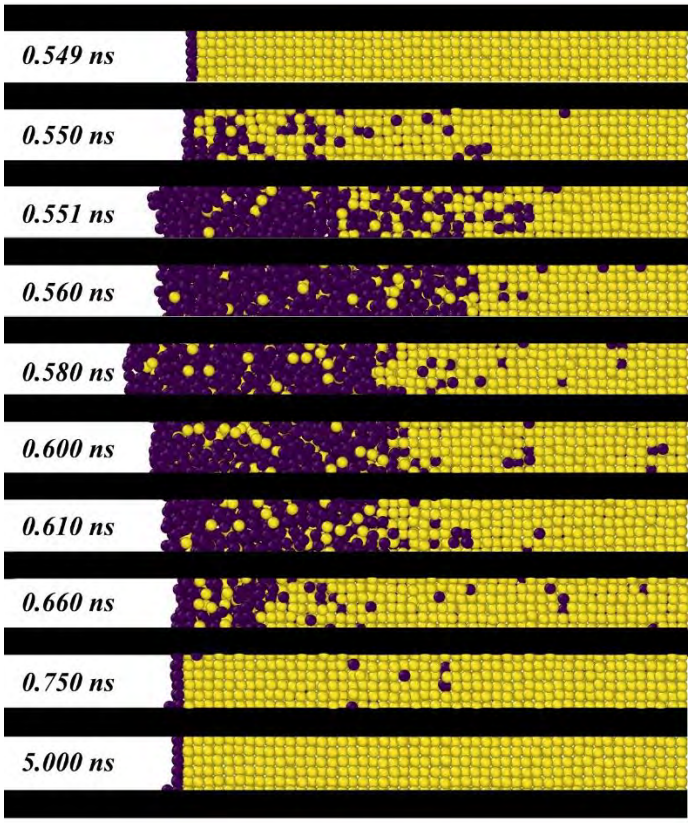

Fig. 3 Ackland analysis at given time. (For the best interpretation of the calculated results, color version of this figure is seen online.)

The analyzed results at given time are shown in Fig. 3, which draws aluminum atoms in the location range $x < 50$ nm. Namely, an approximate depth of 10 nm beneath the front surface is shown in Fig. 3. The liquid and solid phases are characterized in dark and light, respectively. According to the result in [21], melting temperature calculated by the EAM potential implemented in this paper is 1042 K. As seen in Fig. 3, the liquid region becomes larger and larger with the progress of laser irradiation from 0.549 ns to 0.56 ns, which agrees with the deeper temperature evolution along x-direction in Fig. 2. Laser melting further induces thermal expansion of the front surface. Since atoms in the rear deeper region below the melted region are still cold, the interatomic collisions result in heating up of cold atoms. Meanwhile, hot atoms in the localized region get cooled down and resolidified. As seen in Fig. 3, the melting develops rapidly from 0.549 ns to 0.551 ns. Whereas, the resolidification is a much slower process in a time scale around 0.01 ns. Comparing with the initial thickness of the aluminum

film, a minor front surface expansion of the finally resolidified film is observed in Fig. 3.

Evolution of Diffraction Profiles from Atomic Configuration

The diffraction profiles contain detailed information on thermodynamic mechanism of ultrafast laser induced structure change. On the basis of atomic configuration at each MD time step, scattering patterns are interpreted by calculating static structure factors. A sample containing atoms in the region $x < 45\ nm$ was taken into account in this paper. The temporal evolution of structure factor is seen in Fig. 4, which was calculated from Eq. (4)

$$S(q) = 1 + 4\pi\rho \int_0^\infty \frac{\sin(qr)}{qr} r^2 [g(r) - 1] dr, \qquad (4)$$

where ρ is the number density. The scattering vector, position of atom and pair correlation function are denoted as q, r and $g(r)$, respectively. As seen in Fig. 4, there is a significant transformation of the structure factor from $0.549\ ns$ (before laser irradiation) to $0.56\ ns$ (right after laser irradiation), which results from the ultrafast laser heating of the aluminum atoms in femtoseconds time scale.

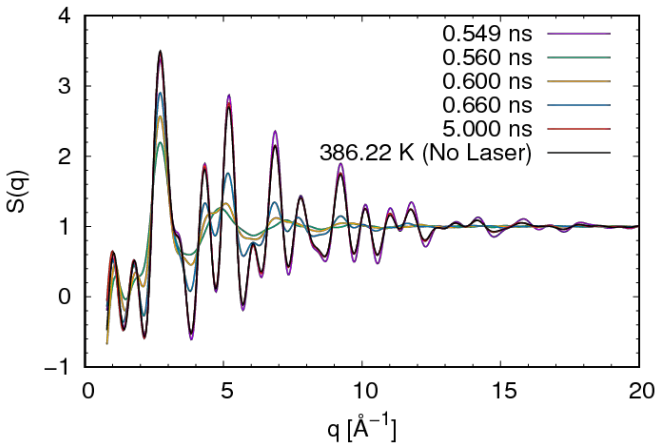

Fig. 4 Evolution of structure factor *S(q)* at given time. (For the best interpretation of the calculated results, color version of this figure is seen online.)

Comparing with solid crystalline, liquid phase does not show long range order. Therefore, there are no obvious sharp peaks and valleys of structure factor in $q > 10$ Å^{-1} from $0.56\ ns$ to $0.66\ ns$ in Fig. 4. Moreover, for short range order ($q < 10$ Å^{-1}), there are peaks and valleys with smaller magnitudes for the cases when $0.56\ ns < t < 0.66\ ns$ than the case at $0.549\ ns$. Recalling the results of Ackland analysis in Fig. 3, the case with larger proportion of liquid phase presents smaller magnitudes of peaks and valleys in Fig. 4. Additionally, at high scattering vector q, the structure factor $S(q)$ of laser melting region goes to 1, which is verified by the results at $q = 20$ Å^{-1} in Fig. 4. As seen from the magnitudes of peaks and valleys when 5 Å$^{-1} < q < 15$ Å^{-1}, even though the melted region becomes resolidificated at the end of simulation, there are slight discrepancies between the final structure factor at $5\ ns$ and that before laser irradiation at $0.549\ ns$. Besides the simulation of laser irradiation, another case without laser irradiation was performed in terms of canonical NVT ensemble at a temperature ($386.22\ K$) equal to the laser irradiated case at $5\ ns$, whose structure factor was calculated and plotted in Fig. 4 as well. It can be seen that the two structure factors (at 5 ns and at 386.22 K without laser irradiation) overlap together, which indicates the two diffraction profiles are the same. Therefore, it can be concluded that difference between the structure factors at $0.549\ ns$ and at $5\ ns$ comes from different temperatures of the two states.

CONCLUSIONS

To sum up, phase change phenomena of melting and resolidification induced by ultrafast laser heating are studied by MD simulation in this paper. The following conclusions are drawn:

(1) An abrupt temperature increase of the laser penetrated region happens upon laser pulse irradiation. The thermal conduction process goes slower than the accumulation of laser energy deposition, resulting in localized laser heating beneath the laser irradiated surface.

(2) Ackland analysis shows the propagation of liquid-solid interface during laser melting is much faster than that during resolidification. Therefore, it can be derived that the timescale of interatomic collision is longer than the duration of ultrafast laser pulse.

(3) Ultrafast laser heating contributes to thermal expansion of the front side of the aluminum film. While, the subsequent resolidification leads to shrink of the expanded front surface. The final thickness of the laser heated film is slightly thicker than that before laser irradiation, because of ultrafast laser irradiation and higher final temperature.

(4) Ultrafast laser irradiation pronouncedly modifies the diffraction profiles in the melted region and slightly changes the structure factor of the aluminum film after resolidification. Owing to the temperature increase after laser energy deposition, diffraction profile of the resolidified aluminum is found different from the aluminum before laser irradiation. Whereas, the resolidified region recover to FCC lattice structure reflected from the Ackland analysis.

ACKNOWLEDGMENTS

Support for this work by the National Natural Science Foundation of China under grant number 51575305, U1537202, 2015B010132005 and 2016YFB1100700, the U.S. National Science Foundation under grant number CBET-133611, the Southern University of Science and Technology Presidential Postdoctoral Fellowship and the Postdoctoral Science Foundation of China under grant number 2017M612653 are gratefully acknowledged.

REFERENCES

[1] Feng, Q., Picard, Y. N., Liu, H., Yalisove, S. M., Mourou, G., and Pollock, T. M., 2005, "Femtosecond Laser Micromachining of a Single-Crystal Superalloy," Scr. Mater., **53**(5), pp. 511–516.

[2] Kim, J., and Na, S., 2007, "Metal Thin Film Ablation with Femtosecond Pulsed Laser," Opt. Laser Technol., **39**(7), pp. 1443–1448.
[3] Yang, C., Wang, Y., and Xu, X., 2012, "Molecular Dynamics Studies of Ultrafast Laser-Induced Phase and Structural Change in Crystalline Silicon," Int. J. Heat Mass Transf., **55**(21–22), pp. 6060–6066.
[4] Mao, Y., and Xu, M., 2015, "Lattice Boltzmann Numerical Analysis of Heat Transfer in Nano-Scale Silicon Films Induced by Ultra-Fast Laser Heating," Int. J. Therm. Sci., **89**, pp. 210–221.
[5] Ou, Z., Huang, M., and Zhao, F., 2016, "The Fluence Threshold of Femtosecond Laser Blackening of Metals: The Effect of Laser-Induced Ripples," Opt. Laser Technol., **79**, pp. 79–87.
[6] Ji, P., and Zhang, Y., 2013, "Femtosecond Laser Processing of Germanium: An Ab Initio Molecular Dynamics Study," J. Phys. D. Appl. Phys., **46**, p. 495108.
[7] Bévillon, E., Colombier, J. P., Dutta, B., and Stoian, R., 2015, "Ab Initio Nonequilibrium Thermodynamic and Transport Properties of Ultrafast Laser Irradiated 316L Stainless Steel," J. Phys. Chem. C, **119**(21), pp. 11438–11446.
[8] Sen, S., and Dickinson, J. E., 2003, "Ab Initio Molecular Dynamics Simulation of Femtosecond Laser-Induced Structural Modification in Vitreous Silica," Phys. Rev. B, **68**(21), p. 214204.
[9] Bizi-Bandoki, P., Benayoun, S., Valette, S., Beaugiraud, B., and Audouard, E., 2011, "Modifications of Roughness and Wettability Properties of Metals Induced by Femtosecond Laser Treatment," Appl. Surf. Sci., **257**(12), pp. 5213–5218.
[10] Ji, P., and Zhang, Y., 2017, "Multiscale Modeling of Femtosecond Laser Irradiation on Copper Film with Electron Thermal Conductivity from Ab Initio Calculation," Numer. Heat Transf. Part A Appl., **71**(2), pp. 128–136.
[11] Ji, P., and Zhang, Y., 2016, "Continuum-Atomistic Simulation of Picosecond Laser Heating of Copper with Electron Heat Capacity from Ab Initio Calculation," Chem. Phys. Lett., **648**, pp. 109–113.
[12] Ji, P., and Zhang, Y., 2017, "Electron–Phonon Coupled Heat Transfer and Thermal Response Induced by Femtosecond Laser Heating of Gold," J. Heat Transfer, **139**(5), pp. 52001–52006.
[13] Ji, P., and Zhang, Y., 2016, "Ab Initio Determination of Effective Electron–phonon Coupling Factor in Copper," Phys. Lett. A, **380**(17), pp. 1551–1555.
[14] Sonntag, S., Paredes, C. T., Roth, J., and Trebin, H. R., 2011, "Molecular Dynamics Simulations of Cluster Distribution from Femtosecond Laser Ablation in Aluminum," Appl. Phys. A Mater. Sci. Process., **104**(2), pp. 559–565.
[15] Fisher, D., Fraenkel, M., Henis, Z., Moshe, E., and Eliezer, S., 2001, "Interband and Intraband (Drude) Contributions to Femtosecond Laser Absorption in Aluminum," Phys. Rev. E, **65**(1), p. 16409.
[16] Siwick, B. J., Dwyer, J. R., Jordan, R. E., and Miller, R. J. D., 2003, "An Atomic-Level View of Melting Using Femtosecond Electron Diffraction," Science, **302**(5649), pp. 1382–1385.
[17] Lin, Z., Zhigilei, L. V., and Celli, V., 2008, "Electron-Phonon Coupling and Electron Heat Capacity of Metals under Conditions of Strong Electron-Phonon Nonequilibrium," Phys. Rev. B, **77**(7), p. 75133.
[18] Sonntag, S., Roth, J., Gaehler, F., and Trebin, H. R., 2009, "Femtosecond Laser Ablation of Aluminium," Appl. Surf. Sci., **255**(24), pp. 9742–9744.
[19] Gruzdev, V., Ji, P., Chen, J. K., Cooper, B., and Zhang, Y., 2015, "Nanostructuring of Rough Aluminum Surface by Ultrashort Laser Pulses : Influence of Laser Fluence," *Conference on Lasers and Electro-Optics (CLEO)*, pp. 3–4.
[20] Verlet, L., 1967, "Computer 'Experiments' on Classical Fluids. I. Thermodynamical Properties of Lennard-Jones Molecules," Phys. Rev., **159**(1), pp. 98–103.
[21] Purja Pun, G. P., and Mishin, Y., 2009, "Development of an Interatomic Potential for the Ni-Al System," Philos. Mag., **89**(34–36), pp. 3245–3267.
[22] Ji, P., Zhang, Y., and Yang, M., 2013, "Structural, Dynamic, and Vibrational Properties during Heat Transfer in Si/Ge Superlattices: A Car-Parrinello Molecular Dynamics Study," J. Appl. Phys., **114**(23), p. 234905.
[23] Plimpton, S., 1995, "Fast Parallel Algorithms for Short-Range Molecular Dynamics," J. Comput. Phys., **117**, pp. 1–42.
[24] Ackland, G. J., and Jones, A. P., 2006, "Applications of Local Crystal Structure Measures in Experiment and Simulation," Phys. Rev. B, **73**(5), pp. 1–7.